pp 651–674. © Royal Aeronautical Society 2016
doi: 10.1017/aer.2016.14

Simulation study of wake encounters with straight and deformed vortices

D. Vechtel
dennis.vechtel@dlr.de
Department of Flight Dynamics and Simulation
DLR German Aerospace Center
Institute of Flight Systems
Braunschweig
Germany

ABSTRACT

A simulation study was conducted in order to investigate the influence of vortex deformation on wake encounter characteristics. Wake vortices tend to be strongly deformed during the decay process, depending on the atmospheric conditions in terms of turbulence and thermal stratification. For quantification of the influence of vortex deformation, encounters of an aircraft of the 'Medium' category behind a generator aircraft of the 'Heavy' category were simulated with straight vortices and with realistically deformed vortices derived from large-eddy simulations. All relevant parameters that influence the encounter characteristics, such as encounter angles and positions, were varied within a wide range. In order to cover all kinds of vortex deformation, encounters with different vortex ages from 16-136 seconds were simulated. Hence, all relevant phases during the vortex decay from nearly straight and wavy vortices to vortex rings were considered.

The parameter variation study revealed that on average the impact on the encountering aircraft is less with deformed vortices than with straight vortices of comparable strength. Especially with vortex rings, the encountering aircraft is exposed to a much smaller impact. However, the results also show a larger aircraft response during encounters with wavy vortices just prior to vortex linking. The maximum aircraft response with wavy vortices is stronger than with straight vortices of comparable strength. Also, the strongest encounters occur under greater encounter angles with deformed vortices than with straight ones.

Keywords: Vortex deformation; hazard assessment; encounter simulation

Received 14 March 2014; revised 23 April 2015; accepted 17 September 2015.

NOMENCLATURE

AIM	aerodynamic interaction model
ATRA	Advanced Technologies Research Aircraft
ATTAS	Advanced Technologies Testing Aircraft System
DLR	German Aerospace Center
DME	distance measurement equipment
ICAO	International Civil Aviation Organisation
ILS	instrument landing system
LES	large-eddy simulation
MAC	mean aerodynamic chord
NDB	non-directional beacon
RCR	roll control ratio
VFW	Vereinigte Flugwerke
VOR	VHF omnidirectional radio range
b_0	initial vortex spacing (m)
B	wing span (m)
$C_{\ell,\mathrm{ind}}$	rolling moment coefficient induced during wake encounter (-)
$C_{\ell,\xi_{\max}}$	rolling moment coefficient due to maximum roll control deflection (-)
C_L	lift coefficient (-)
$C_{L\alpha}$	lift curve slope (1/rad)
C_Y	side force coefficient (-)
$C_{Y\beta}$	side force gradient with respect to sideslip angle (1/rad)
n_z	vertical load factor (-)
p	roll rate (°/s)
r	radial distance from vortex core (m)
r	yaw rate (°/s)
r_c	vortex core radius (m)
t	time (s)
t_{age}	vortex age (s)
t^*	normalised vortex age (-)
u, v, w	velocity components (m/s)
V_T	tangential velocity (m/s)
x, y, z	spatial position in vortex axis (m)
α	angle-of-attack (°)
β	sideslip angle (°)
γ	flight path angle (°)
ε	downwash angle (°)
ε	relation factor (%)
φ	sweep angle (°)
ν	dihedral (°)
ξ	aileron deflection (°)
Γ	vortex circulation (m^2/s)
Γ_0	initial vortex circulation (m^2/s)
Φ	bank angle (°)
Ψ	azimuth (°)
Θ	pitch angle (°)

https://doi.org/10.1017/aer.2016.14 Published online by Cambridge University Press

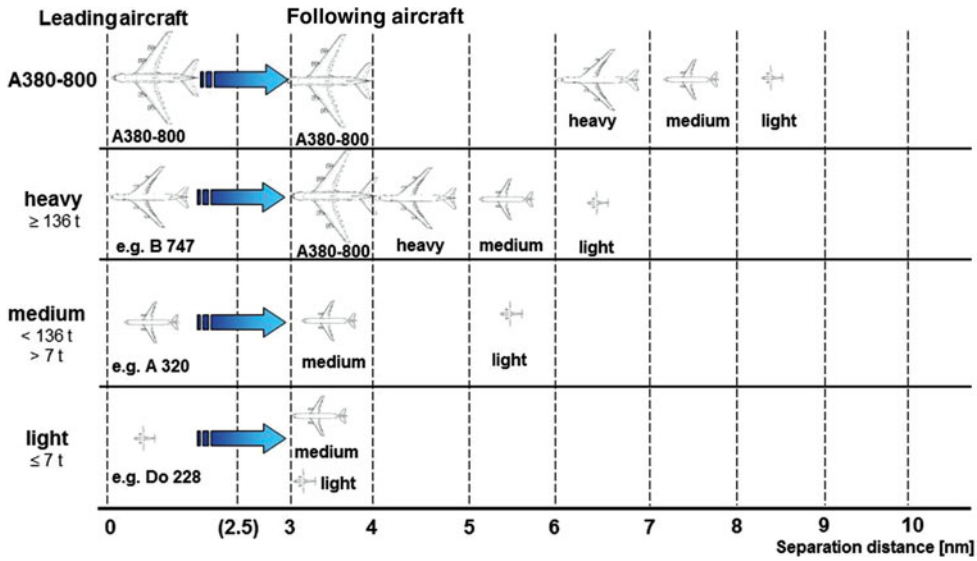

Figure 1. (Colour online) Current ICAO wake turbulence separation minima[3].

1.0 INTRODUCTION

Wake vortices, which are an inevitable result of lift generation, generally pose a threat to aviation because the impact of a wake encounter may lead to a rapid aircraft response such as rolling motion or strong vertical accelerations. In order to avoid hazardous wake encounters, different minimum separation distances were defined in the past. These were designed such that the vortices of a preceding aircraft are suitably decayed when a trailing aircraft may encounter them. Several similar wake vortex related separation schemes exist at present, of which the most widely used one is the one defined by ICAO[1] (Fig. 1). However, in some countries (e.g. the USA and the UK), separation schemes were independently defined and are slightly different from the ICAO scheme. Furthermore, some airports use slightly adapted separation schemes. All of these separation schemes have proven over the last decades to sufficiently prevent hazardous wake encounters and therefore to be acceptably safe. Nevertheless, a noticeable number of wake encounters occur even under today's separation limits; fortunately, encounters with unwanted consequences (such as injuries) are rare[2].

As today's air traffic grows significantly, the present separation schemes begin to limit airport and airspace capacity[3,4]. Furthermore, it is widely accepted that the current separations are overly conservative under many circumstances. As a result, an attempt is here made to revise the existing separation schemes. However, any revision of separations must not lead to an increase in hazardous wake encounters or generally affect aviation safety adversely. In order to quantify the impact on aviation safety due to a revision of separations, the possible hazard of a wake encounter must be assessed. This includes a thorough knowledge of vortex evolution and decay and their effects on the impact on the encountering aircraft.

Wake vortex evolution and decay has been comprehensively investigated[5] in the past, and a mature knowledge now exists concerning vortex behaviour during its decay in terms of the evolution of quantities such as vortex circulation, core radius, radial velocity profile, etc. However, one effect often neglected is the vortex deformation, which evolves during the decay.

https://doi.org/10.1017/aer.2016.14 Published online by Cambridge University Press

Figure 2. (Colour online) Vortex deformation during decay[9]. (Photo: DLR).

Similar to most other quantities affected by the decay, the evolution of the vortex deformation strongly depends on the atmospheric conditions. Atmospheric conditions such as turbulence and thermal stratification lead to deformations, which can be divided into several distinct phases (Fig. 2). After their creation, the vortices are more or less straight (phase 1). After some time, one can observe the onset of the so-called Crow instability (phase 2), which is the key driver for vortex deformation, and is followed by a phase with increasing deformation (phase 3). In this phase, the vortices begin to form a sinusoidal shape with increasing amplitude. As a result such deformed vortices are often called 'wavy vortices'. Finally, the vortices link at intervals to form a chain of vortex rings (phase 4).

Although a lot of scientific work on wake vortices in general was performed in the 1950s and 1960s, the effect of vortex deformation was first investigated in 1970 by Crow[6], after whom the instability was named. Crow also investigated the lifetime of deformed vortices and the time span until vortex linking[7]. However, the way in which the encounter hazard is affected by vortex deformation was first analysed by Loucel and Crouch in 2004[8]. Until then, the effect of vortex deformation was known to exist, but was mostly neglected for wake encounter hazard analysis. Most encounter hazard assessment studies assumed the wake to consist of two counter-rotating infinitely long and straight vortices[5]. However, recent studies revealed that vortex deformation might have a considerable influence on the subjective perception of a threat during a wake encounter from a pilot's perspective[9-11]. All previous studies concluded that no final statement can be made about this topic and that further research needs to be performed. There is still no clear understanding on whether or not wake encounters with deformed vortices are more hazardous than those with straight vortices.

In order to gain more insight in the effects of vortex deformation on the encounter characteristics, a simulation study was conducted using a simulation model of the DLR research aircraft A320 ATRA (Advanced Technologies Research Aircraft) and different realistic flow fields derived from large-eddy simulations (LES) representing all the relevant effects during vortex decay. This paper presents the outcomes of this simulation study. First of all, the simulation is described in terms of the aircraft model, the flight control system, the wake vortex models and the aerodynamic interaction model. Finally, simulation results are presented.

2.0 SIMULATION

The simulations were performed using existing models of the encountering aircraft[12], the wake vortices[13], and the aerodynamic impact of the vortex flow field on the encountering aircraft[14]. All parts were combined in one Simulink® model, which includes the model of the encountering aircraft with a flight control system and autopilot, the analytical model of the straight vortices, the LES- derived datasets of the deformed vortices and the aerodynamic interaction model (which calculates the vortex-induced forces and moments acting on the encountering aircraft). The encounters were simulated space-fixed, which means that the

https://doi.org/10.1017/aer.2016.14 Published online by Cambridge University Press

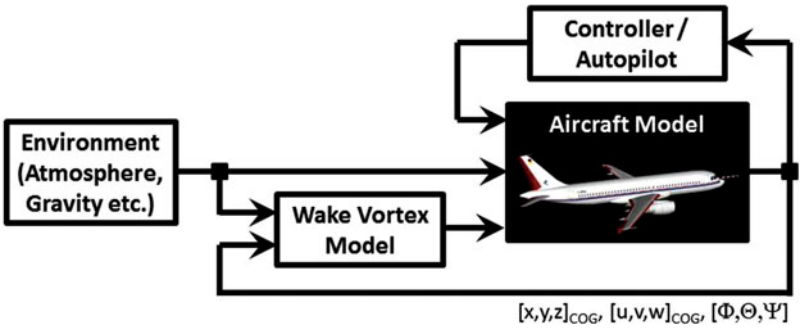

Figure 3. (Colour online) Overall simulation model architecture.

vortices were fixed in space and the encountering aircraft flew through the vortices on a free flight path. As the duration of the encounter was usually quite short, wind drift and sinking of the vortices were small in comparison to the aircraft's airspeed and hence can be neglected. Therefore, the assumption of the vortices being fixed in space appears reasonable. This method is considered to realistically represent the wake's influence on the aircraft's flight path. Here it is noted that the encountering aircraft's influence on the vortex flow field is neglected.

The overall architecture of the simulation is shown in Fig. 3. The Simulink® model is embedded in the simulation control developed in Matlab®. The environment model includes the calculation of the gravity, the atmospheric conditions (air pressure and density, temperature, etc.), wind and turbulence. However, wind and turbulence was disabled for the simulation study presented here. The following sections briefly describe each part of the simulation to give an overview on the models used and the reliability of the simulation results.

2.1 Aircraft model

The DLR research aircraft ATRA, an Airbus A320 (Fig. 4), was chosen as the encountering aircraft for the simulations, as it represents a typical airliner in widespread use for which the DLR Institute of Flight Systems possesses a very accurate simulation model. The simulation model was developed after ATRA came into service at DLR in 2006. The entire model has been continuously upgraded since then by the DLR Institute of Flight Systems and has been identified and validated from real flight data gathered from several flight tests campaigns. As the model is validated using data from real aircraft which has been continuously updated, the confidence in the model accuracy is good[12].

Besides the equations of motion and the calculation of weight and balance, the aircraft model comprises an aerodynamic model, a propulsion model of the IAE V2500 engines, a landing gear model, sensor models of the radio altimeters, air data system (pressure sensors, wind vanes, etc.), inertial reference system and navigation sensors (DME, NDB, VOR, ILS, etc.), as well as simplified actuator models for all control surfaces (second-order actuators with time delay). The aerodynamic model is based on stability and control derivatives identified from flight test data including non-linear corrections for dynamic pressure and Mach number effects. Mach number effects are represented by the Prandtl-Glauert factor. Furthermore, a stall model and ground effect is included. For longitudinal motion, the aerodynamics are split into two parts (the fuselage/wing and the tail), whereas for lateral motion, a one-point-model is used. The model is valid within the normal operational flight envelope. At the boundaries of the flight envelope, the model accuracy might decrease. The model is used for a

https://doi.org/10.1017/aer.2016.14 Published online by Cambridge University Press

Figure 4. (Colour online) The DLR research aircraft ATRA. (Photo: D. Vechtel).

motion-based full-flight simulator operated by the DLR Institute of Flight Systems but can also be used for offline simulations on regular personal computers. The aircraft model accuracy is considered to be acceptable for scientific simulation purposes. Most requirements for pilot training simulations are met by the model within the tolerance range[12,15].

2.2 Flight control system and autopilot

The flight simulation used in this study includes a flight control system, which comprises a direct and a normal law for manual flight as well as an autopilot for automatic flight. The design of the controllers was based on the Airbus flight control system philosophy. All flight modes of the A320 were implemented. The autopilot comprises all possible modes for automatic flight of the A320 using selected command values (such as altitude acquire and hold, heading/track acquire and hold, open descent and climb or descent/climb with selected vertical speed, etc.) but also enables managed flight based on flight-plan-related command values. In this study, none of the manual flight control laws were used, but the wake encounters were simulated using the autopilot in altitude and heading hold mode.

Contrary to the aircraft model, the flight control system and the autopilot cannot directly be validated by means of flight test data. The behaviour of the control system on a specific control input is indeed validated by means of flight test data of the real aircraft, but the correct response on an external disturbance (such as gusts or wake turbulence) can only be validated if the disturbance is known as well. Such data are still not available to DLR. Hence, the development of the flight control system for the ATRA simulation was mainly based on manuals available to aircraft operators[16,17]. The validation of the autopilot response to control inputs shows good conformity with the behaviour of the real autopilot. However, the simulation results show that the aircraft response on the wake encounter is realistic and can be considered to be representative.

2.3 Vortex simulation and aerodynamic interaction model

Besides the accurate models of the aircraft and autopilot, the wake vortex simulation is one of the most important parts of the simulation. This includes not only the accurate modelling of the vortex flow field but also the modelling of the aerodynamic interaction between the vortices and the aircraft, namely the calculation of vortex-induced forces and moments.

https://doi.org/10.1017/aer.2016.14 Published online by Cambridge University Press

In this study for both, straight and deformed vortices, the generator aircraft is an aircraft in the 'Heavy' category in approach configuration with a gross weight of 190 tons, a wingspan of 60.3 m and airspeed of 72 m/s, which is a typical approach speed for such an aircraft. The altitude is not relevant for the LES, but the air density was set to 1.225 kg/m^3. The encounter simulations were performed at an altitude of 4,000 ft.

2.3.1 Model of straight vortices

The straight vortices were modelled using the model of the radial distribution of tangential velocity by Burnham and Hallock[18], or Rosenhead[19] respectively. The vortex-induced forces and moments were calculated by superimposing two single, counter-rotating, straight and infinitely long vortices. This analytical model was used at DLR Institute of Flight Systems for various wake vortex simulations and the experience with this model to sufficiently represent a realistic radial velocity distribution is good[20]. The tangential velocity of a vortex of infinite length to both sides is calculated by

$$V_T(t,r) = \frac{\Gamma(t)}{2\pi}\frac{r}{r^2 + {r_c}^2}, \quad \ldots(1)$$

with the time dependent vortex circulation Γ, the core radius r_c (at which the tangential velocity has its maximum) and the radial distance from the vortex centre r. Based on values identified from flight tests by Fischenberg[20] the core radius was set to $0.035 \times b_0$ for all vortex ages. The initial vortex spacing b_0 can be estimated to be $\pi/4 \times B$ (with the wing span B) if the lift distribution is assumed to be elliptical. The value for the core radius was identified in flight tests with the research aircraft of the Technical University Braunschweig (Dornier Do 128-6), which encountered the wake of the former DLR research aircraft ATTAS (VFW 614) and measured the vortex flow field with four five-hole probes. For this specific generator aircraft, the core radius is about 29% of the mean aerodynamic chord. In reality, the core radius grows during the vortex decay, but this effect was neglected here, as the core radius is typically set to a fixed value regardless the vortex age in encounter simulation studies[8,11,21]. In order to simulate encounters with wake vortices of comparable strength the circulation of the straight vortices was taken from the average circulation of the LES vortices for each vortex age, so that vortex decay is covered for the simulations with straight vortices.

2.3.2 Deformed vortices from large-eddy simulations

The flow fields used for the encounters with deformed vortices were generated by large-eddy simulations (LES). These LES were conducted by the DLR Institute of Atmospheric Physics within the frame of a DLR-internal project called 'Weather and Flying' between 2008 and 2011[22].

The atmospheric conditions which were applied for the LES used in this study were moderate turbulence and neutral thermal stratification, which are reasonable values for the lower layer of the atmosphere[23]. Compared to other atmospheric conditions in terms of turbulence and thermal stratification the chosen conditions result in not too fast decay and more or less symmetrical deformation (contrary to for example, stable thermal stratification and strong turbulence, which result in quickly decayed and arbitrarily deformed vortices). Therefore, these atmospheric conditions are considered to be useful for the desired purpose of the presented simulation study.

Figure 5 presents some results of the LES at different vortex ages, namely one nearly straight vortex pair right after creation ($t_{age} = 16$ s), two in the stage of wavy vortices with

https://doi.org/10.1017/aer.2016.14 Published online by Cambridge University Press

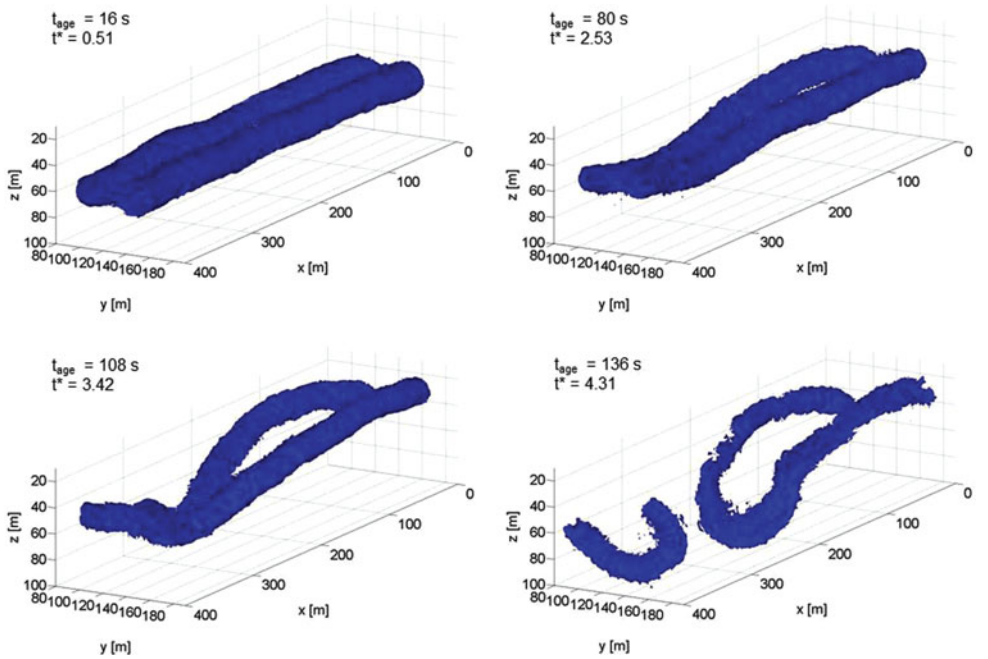

Figure 5. (Colour online) Iso-surfaces of a flow velocity of 6 m/s at different vortex ages.

increasing amplitude ($t_{age} = 80$ s and $t_{age} = 108$ s) and one in the stage of vortex rings ($t_{age} = 136$ s). The figure shows the iso-surfaces of a flow velocity of 6 m/s. The common way to normalise the vortex age is applied here as well:

$$t^* = t_{age} \frac{\Gamma_0}{2\pi \times {b_0}^2} \quad \ldots (2)$$

with the initial vortex spacing b_0 and the initial circulation Γ_0.

The flow fields of the LES were implemented in the simulation as 3D flow fields using lookup tables with a tri-linear interpolation method for the three velocity components u, v and w as a function of the spatial position x, y and z. The spatial resolution of the lookup table data was $1 \times 1 \times 1$ m, which is a resolution of 2.11% of the b_0. The core radius ranges between 3.552 m for the 16-second-old vortices and 5.934 m for the 136-second-old vortices. Hence, the vortex core always includes a sufficient number of data points to be properly represented.

Due to computational limits, the length of the LES domain was set to 400 m. This length is indeed sufficient for the large-eddy simulations as it covers one wavelength of the Crow instability, which is the predominant factor for vortex deformation; however, for wake encounter flight simulation, this length is too short. Therefore, the flow field of one vortex age is connected in series so that in the flight direction of the generator aircraft, an infinitely long flow field is formed with the repeated shape of the oscillating LES vortices. This assumption is valid as long as the airspeeds of both the generating and the encountering aircraft are within a similar range so that the time separation between both aircraft remains the same. In such a case, the trailing aircraft will always encounter vortices of only one age (hence, one degree of deformation), depending on the airspeed of both aircraft and their separation distance.

https://doi.org/10.1017/aer.2016.14 Published online by Cambridge University Press

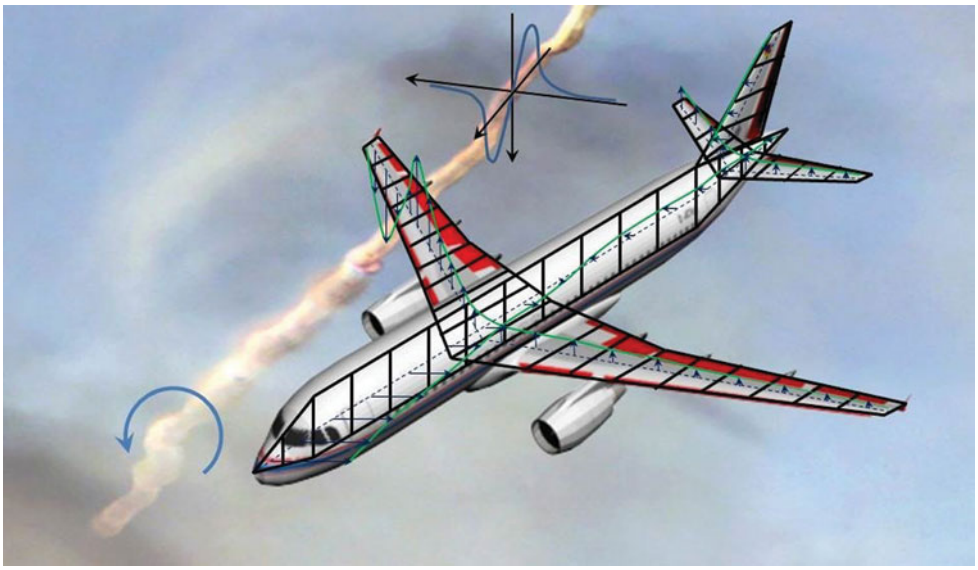

Figure 6. (Colour online) The strip method.

2.3.3 Aerodynamic interaction model

Besides the vortex flow field models, an aerodynamic interaction model (AIM) is needed in order to calculate the vortex-induced forces and moments acting on the encountering aircraft. As the aircraft model already incorporates an accurate aerodynamic model, the AIM used for the encounter simulations is designed as a delta-model calculating only the delta-aerodynamics resulting from the additional angle-of-attack and sideslip angle due to the vortex flow field.

For the AIM, the so-called strip method is used, where the lift and side-force generating surfaces (wings, stabilisers and fuselage) of the encountering aircraft are subdivided into sections for which the vortex influence is determined (Fig. 6). For each strip of a horizontal plane (wings and horizontal stabiliser) and for each strip of a vertical plane (vertical stabiliser and fuselage), an additional angle-of-attack and angle of sideslip is calculated respectively for the vortex flow field velocity components at each respective strip position:

$$\Delta\alpha_{WV,i} = -\frac{v_{WV,i}\times\sin\nu + w_{WV,i}\times\cos\nu}{\sqrt{\left(u_a^b\times\cos\varphi + v_a^b\times\sin\varphi\times\cos\nu - w_a^b\times\sin\varphi\times\sin\nu\right)^2 + \left(v_a^b\times\sin\nu + w_a^b\times\cos\nu\right)^2}} \quad \ldots(3)$$

$$\Delta\beta_{WV,i} = -\frac{v_{WV,i}}{\sqrt{\left(u_a^b\times\cos\varphi - w_a^b\times\sin\varphi\right)^2 + \left(v_{a^b}\right)^2}}, \quad \ldots(4)$$

where the vortex induced flow velocity components at each strip are denoted by $u_{WV,i}$, $v_{WV,i}$ and $w_{WV,i}$, the aerodynamic velocity components at the centre of gravity in body-fixed coordinates are u_a^b, v_a^b and w_a^b, the sweep angle is φ and the dihedral is ν. Both angle-of-attack and sideslip angle are limited to a specific maximum value (e.g., for wing strips, the angle-of-attack is

https://doi.org/10.1017/aer.2016.14 Published online by Cambridge University Press

limited to 20°) in order to prevent unrealistically large forces from being computed. However, a dedicated stall model is not included.

With these additional flow angles due to the vortex flow field at each strip number, the resulting forces acting on each strip are calculated. For strips of horizontal planes, an additional lift force is determined, and for strips of vertical planes, an additional side force is determined. Drag changes due to the local vortex flow velocities are disregarded; for this reason, no longitudinal force is evaluated. The additional lift is calculated for horizontal strips with:

$$\Delta C_{L,WV,i} = C_{L\alpha} \times \Delta\alpha_{WV,i} \times \left(1 - \frac{\partial\varepsilon}{\partial\alpha}\right), \quad \ldots(5)$$

where the lift curve slope is represented by $C_{L\alpha}$, the local change of angle-of-attack due to the vortex flow field $\Delta\alpha_{WV,i}$ and a downwash factor for the horizontal tail $(1 - d\varepsilon/d\alpha)$. For wing strips, the downwash factor of the tail is neglected. This formula is a steady description of the lift. In reality the downwash is indeed influenced by the vortex flow field. Depending on the encounter angles, a wake encounter can be a highly unsteady event. For small encounter angles such as those presented here, the event can be regarded as almost steady (especially in case of straight vortices). Recent studies have shown that unsteady effects can indeed be observed during the wake encounter but are small, as all the local effects are summed up for the whole aircraft[11]. Furthermore, unsteady aerodynamic effects would reduce the aircraft reaction, so for this reason, the approach chosen here can be considered to be conservative.

The additional side force is calculated for vertical strips with:

$$\Delta C_{Y,WV,i} = C_{Y\beta} \times \Delta\beta_{WV,i} \quad \ldots(6)$$

with the side force gradient $C_{Y\beta}$ and the local sideslip angle due to the vortex flow field $\Delta\beta_{WV,i}$. The resulting moments are then calculated with each strip's force and the respective lever arm:

$$\Delta\underline{M} = \underline{r} \times \Delta\underline{F} \quad \ldots(7)$$

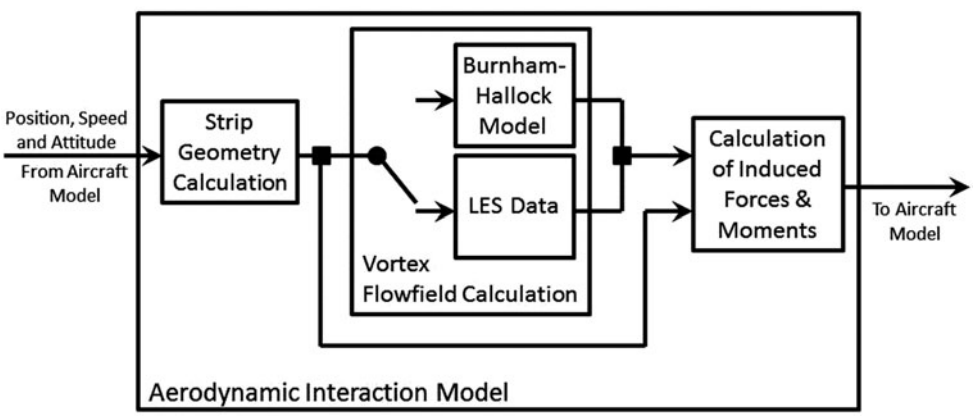

Figure 7. Architecture of the aerodynamic interaction model.

https://doi.org/10.1017/aer.2016.14 Published online by Cambridge University Press

The vortex-induced forces and moments are fed into the equations of motion of the aircraft model.

This method was deemed feasible by Barrows[24], verified against wind tunnel tests by de Bruin[25] and further validated using real flight test data by Fischenberg[20] and Jategaonkar[26].

Figure 7 visualises the general architecture of the AIM used for this simulation. Depending on the current aircraft attitude and inertial position, the position of each strip is evaluated in geodetic coordinates. For each of these strips the current vortex induced flow velocities are then evaluated.

Here, a switch provides the option of choosing whether straight or deformed vortices are encountered. Hence, either the Burnham-Hallock model or the look up tables with the LES data are used. Finally, with the strip positions and the flow velocities acting on each strip, the resulting forces due to additional angle-of-attack and sideslip angle are calculated for each strip as described above.

This method to determine the vortex impact on the encountering aircraft was applied in various studies in the past[9,10,14,21,27] and is accepted to provide vortex induced forces and moments of acceptable accuracy.

2.4 Parameter variation study

With the simulation as described above, a parameter variation study was conducted in order to evaluate differences between encounters with straight and deformed vortices. In order to cover all aspects of vortex deformation, the vortex ages were varied between 16 and 136 seconds, as these suitably cover nearly the whole lifespan of the vortices under the chosen atmospheric conditions. From an operational point of view, many of the investigated vortex ages are outside the normal operating scope because no aircraft will encounter such young vortices in real airline operations. However, as the LES vortices are also more or less straight at very young ages, it is also possible to directly compare the analytical calculation of straight vortices and

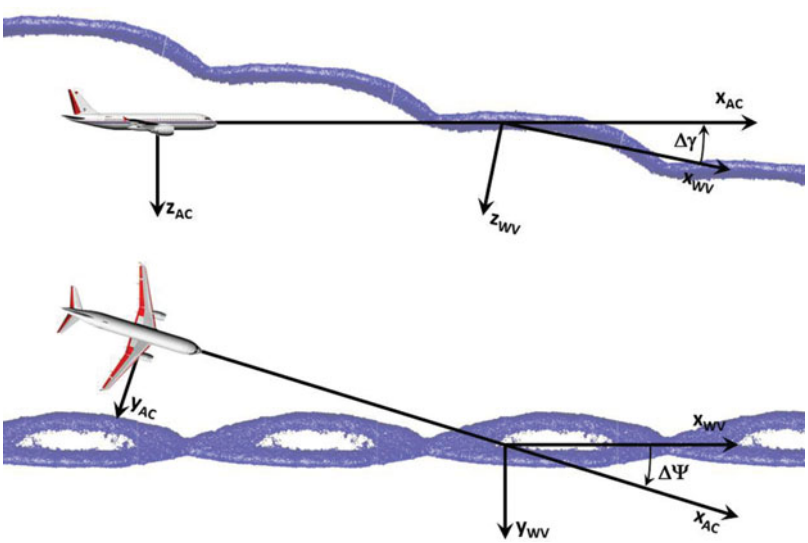

Figure 8. (Colour online) Definition of encounter geometry.

https://doi.org/10.1017/aer.2016.14 Published online by Cambridge University Press

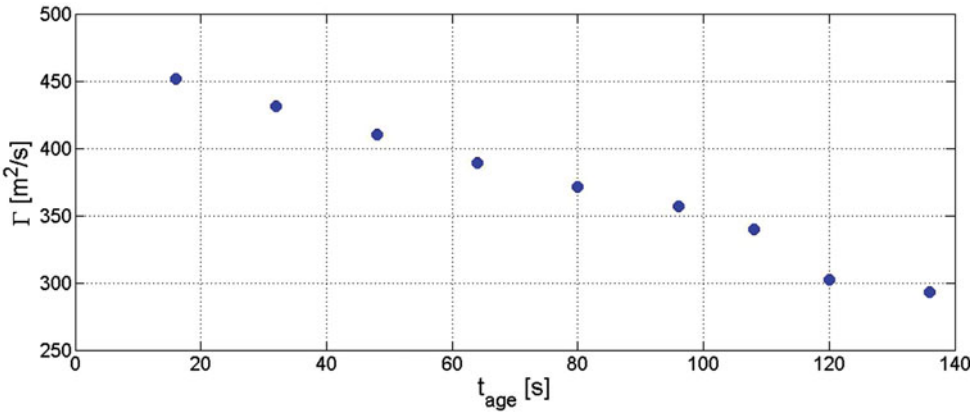

Figure 9. (Colour online) Vortex circulation as applied for the different vortex ages.

the LES vortices. For young vortex ages, both models should result in a similar impact on the encountering aircraft, and with increasing vortex age, the influence of vortex deformation can therefore be evaluated. In order to cover a vast variety of parameter combinations, the main parameters were varied within the following ranges.

The encounter angles are the encounter azimuth $\Delta\Psi$ and the encounter inclination $\Delta\gamma$ (Fig. 8). For the LES vortices, these encounter angles were varied between –15° and 15° for $\Delta\gamma$ (in 1° steps) and between –30° and 30° for $\Delta\Psi$ (in 2° steps). Indeed, symmetry of the vortices could be assumed; however, as the LES vortices might be slightly asymmetrical, the encounter azimuth $\Delta\Psi$ was varied between –30° and 30° in order to find the worst-case encounter conditions. As the encounter does not solely depend on the encounter angles but also on the position where the vortices are crossed as a result, the lateral encounter position Δy was varied between –50 m and 50 m in 10 m steps and the longitudinal encounter position Δx was varied between 0 m and 400 m in 100 m steps. For the deformed vortices, the z-position of the vortex line differs locally due to the vortex deformation. For this reason, the z-position was varied as well for those encounters where $\Delta\gamma = 0$ in order to find the maximum aircraft reaction for this encounter situation.

For the straight vortices, the same range of encounter angles and lateral encounter positions was simulated. However, the straight vortices are indifferent in lateral direction and for this reason, the longitudinal encounter position was not varied for the straight vortices. In order to adapt the straight vortices to the deformed vortices in terms of their strength, the mean circulation of the LES vortices at each vortex age was chosen. The vortex ages and corresponding circulations applied are shown in Fig. 9. All together, almost 500,000 encounters were simulated.

3.0 RESULTS

The evaluation of the simulation results is mainly based on the aircraft response during the encounter. In addition to the aircraft response, one other metric often used for wake encounter hazard assessment is the so-called roll control ratio (RCR)[9,10,27]. The RCR is the ratio between the vortex-induced rolling moment and the maximum rolling moment achievable

https://doi.org/10.1017/aer.2016.14 Published online by Cambridge University Press

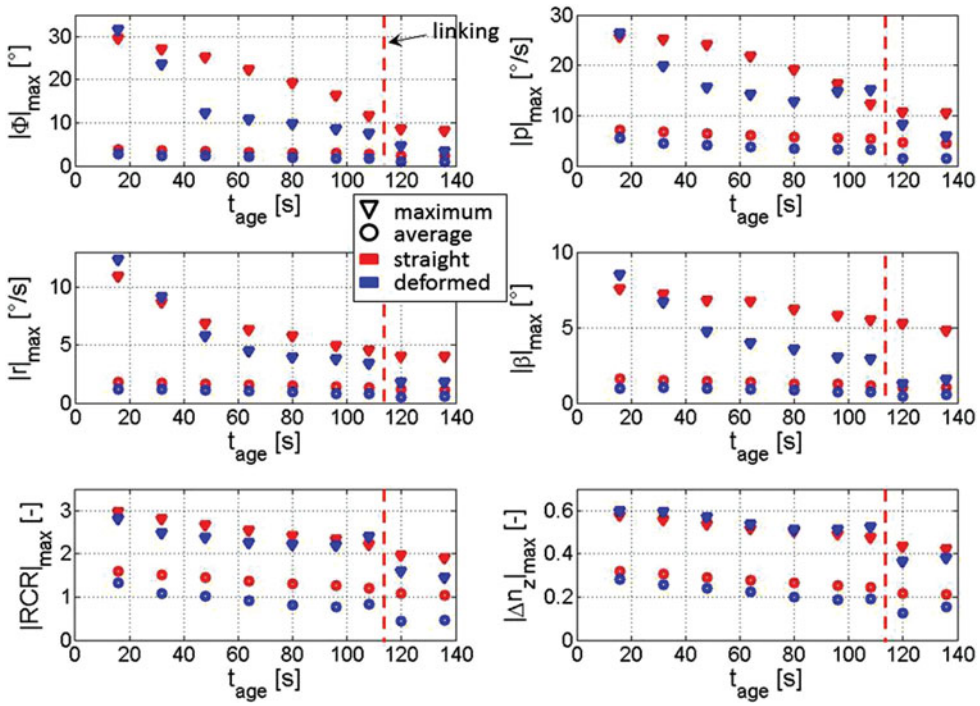

Figure 10. (Colour online) Maximum and average aircraft response as a function of the vortex age.

by a full deflection of all roll control motivators (ailerons, roll spoilers, etc.).

$$RCR = \frac{C_{\ell,\mathrm{ind}}}{C_{\ell,\xi_{\max}}} \qquad \ldots (8)$$

Hence, the RCR is a good measure for the encounter strength and the encountering aircraft's resistance to induced rolling motion. For this reason, it is also shown here alongside parameters describing the aircraft motion.

Figure 10 shows the maximum and average values of the maximum bank angle, maximum roll rate, maximum yaw rate, maximum sideslip angle, maximum RCR and maximum vertical load factor deviation, which all occurred during the wake encounters for straight and deformed vortices as a function of the vortex age. The values for one vortex age include the results of all simulations of that vortex age independently from the encounter geometry. The maximum values shown in Fig. 10 are the overall maxima of all simulations of that age. The average values are the average of the maxima, which occurred during the simulation runs.

Figure 10 illustrates that the average values of all parameters are smaller for deformed vortices than for straight ones. As the number of simulations with deformed vortices is four times higher, this implies that strong encounters occur less frequently with deformed vortices. This issue is further discussed below. Nevertheless, the maximum values of the aircraft response show a quite different tendency than the average. Figure 10 shows that the aircraft response during encounters with deformed vortices decreases quickly with increasing vortex

https://doi.org/10.1017/aer.2016.14 Published online by Cambridge University Press

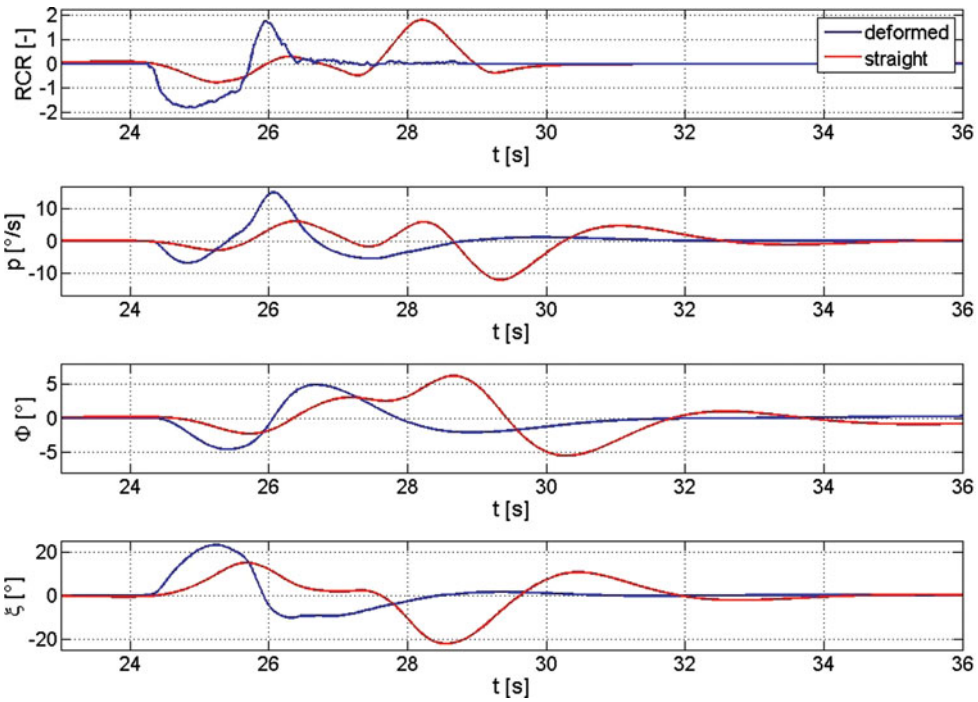

Figure 11. (Colour online) Encounters with maximum roll rate at vortex age of 108 s.

age in comparison to encounters with straight vortices. This fact can be observed especially in the roll axis (bank angle and roll rate) but also for the sideslip angle.

Another fact which can be observed for all parameters is a rapid decrease in aircraft response after the vortex linking (red dashed line). This decrease is not observable with straight vortices and therefore is directly related to either vortex deformation or vortex ring formation, respectively.

However, one of the most astonishing outcomes from Fig. 10 is a temporary increase in the aircraft response in the phase of wavy vortices shortly prior to vortex linking. The simulations with the 108-second-old wavy vortices (Fig. 5) show that such encounters result in even stronger aircraft reaction than with straight vortices of comparable strength. This tendency can be observed for the maximum roll rate, the maximum RCR, and the maximum vertical load factor deviations.

This effect can be explained by analysing the respective encounters with the maximum aircraft response. Figure 11 shows the time histories of roll control ratio RCR, roll rate p, bank angle Φ and aileron deflection ξ commanded by the autopilot, both for the encounters with maximum roll rate with straight and deformed vortices of an age of 108 seconds. In the case of the deformed vortices, the encounter with the maximum roll rate occurred at an encounter azimuth of 16°, whereas the encounter with maximum roll rate and straight vortices occurred at 12° of azimuth (Figs. 12 and 13, both top views). The encounter inclination angle differs more significantly between encounters with straight and deformed vortices. While the encounter with maximum roll rate and straight vortices occurred at a very small encounter inclination angle of −3°, this angle was much larger in the case of deformed vortices, namely 13° (Figs. 12 and 13, both side views). This shows that the encounter situation leading to the

https://doi.org/10.1017/aer.2016.14 Published online by Cambridge University Press

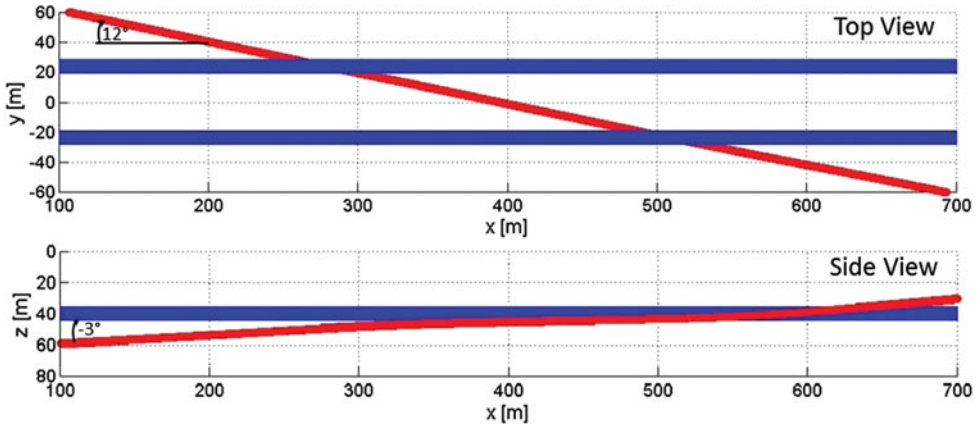

Figure 12. (Colour online) Flight path with maximum roll rate at vortex age of 108 s (straight vortices).

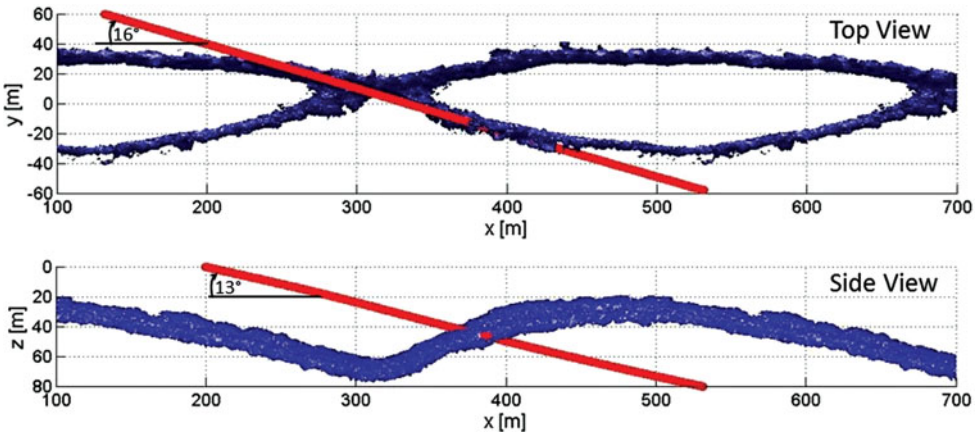

Figure 13. (Colour online) Flight path with maximum roll rate at vortex age of 108 s (deformed vortices).

largest aircraft response is totally different for straight and deformed vortices. With straight vortices, the aircraft approaches the vortices from aside and slightly from below (Fig. 12), whereas with deformed vortices, the aircraft approaches the vortices with a comparable azimuth, but in a steep descent from above (Fig. 13).

Figures 12 and 13 clearly show how different the encounters are. With straight vortices, the aircraft flies below the port vortex and then hits the starboard vortex under shallow angles. This is why the roll impact is stronger during the encounter of the starboard vortex (Fig. 11). With the deformed vortices, the aircraft first flies along the vortex line for quite a long time so that a large rolling moment is induced over a relatively long period of time. Finally, the aircraft crosses the vortex line directly, but due to the vortex deformation, the local encounter inclination is a lot larger than with straight vortices, so the overall encounter duration is actually shorter with deformed vortices; nevertheless, the gradients of the vortex impact are larger. In general terms, the differences between encounters with straight and deformed vortices seem to be the only result of the different encounter geometry in terms of flight path and vortex line position.

https://doi.org/10.1017/aer.2016.14 Published online by Cambridge University Press

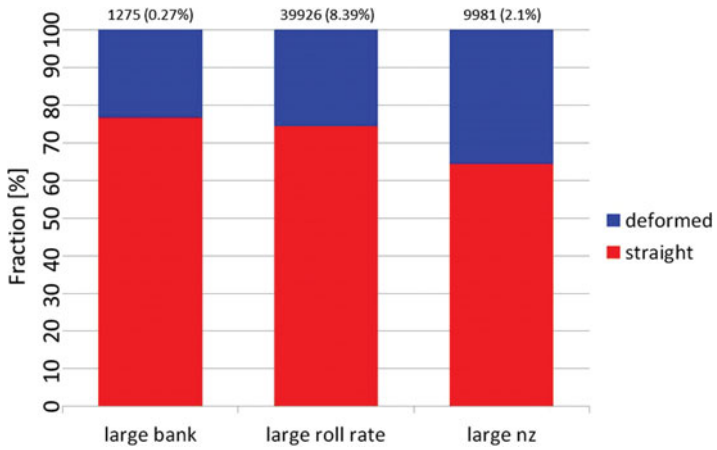

Figure 14. (Colour online) Amount of encounters with large bank angles (>10°), large roll rates (>10°/s) or large vertical load factors (>1.5 or <0.5) (all vortex ages).

The wide spread between the maximum and average values in Fig. 10 indicates that only a small number of encounters occurred with a significant aircraft response to the wake impact. It is obvious that within the wide range of variations, most parameter combinations result in none or only weak encounters.

In order to prevent a possible underestimation of the aircraft response by looking at the average values, Fig. 14 shows the distribution of encounters with straight and deformed vortices during which large bank angles (>10°), large roll rates (>10°/s) or large vertical load factors (>1.5 or <0.5) occurred. The value depicted on top of each column is the amount of encounters during which the respective parameter exceeded the above mentioned boundary relative to the total amount of all 475,695 simulated encounters.

Figure 14 shows that only in 0.27% of all simulated encounters, bank angles greater than 10° occurred, and only in 2.1%, the vertical load factor exceeded 1.5 or 0.5 g. Roll rates greater than 10°/s occurred in 8.39% of all encounters. However, this only shows the amount of encounters with noticeable aircraft reaction. What is more interesting is the distribution of such encounters between the encounters with straight and deformed vortices. Figure 14 clearly shows that large bank angles and large roll rates as well as large vertical load factors mostly occurred during encounters with straight vortices. Only in about 25% of all encounters, large bank angles or large roll rates occurred with deformed vortices, and in about 35%, large vertical load factors occurred with deformed vortices. However, this total does not distinguish between the different vortex ages.

The interpretation of Figs. 10-14 is that due to the previously mentioned reasons, encounters with wavy vortices may result in larger aircraft reactions than with straight vortices; nevertheless the probability of such strong encounters is smaller than with straight vortices.

In the following, the distribution of the encounter strength within the range of encounter angles is analysed for the different typical vortex shapes, nearly straight (very young) vortices, wavy vortices and vortex rings. Here, the encounters with the simple model of straight vortices serve as a reference. In order to allow a direct comparison between encounters with straight and deformed vortices, the values depicted in the following figures are related to the worst-case encounter with straight vortices with respect to the specific parameter. Hence, the

https://doi.org/10.1017/aer.2016.14 Published online by Cambridge University Press

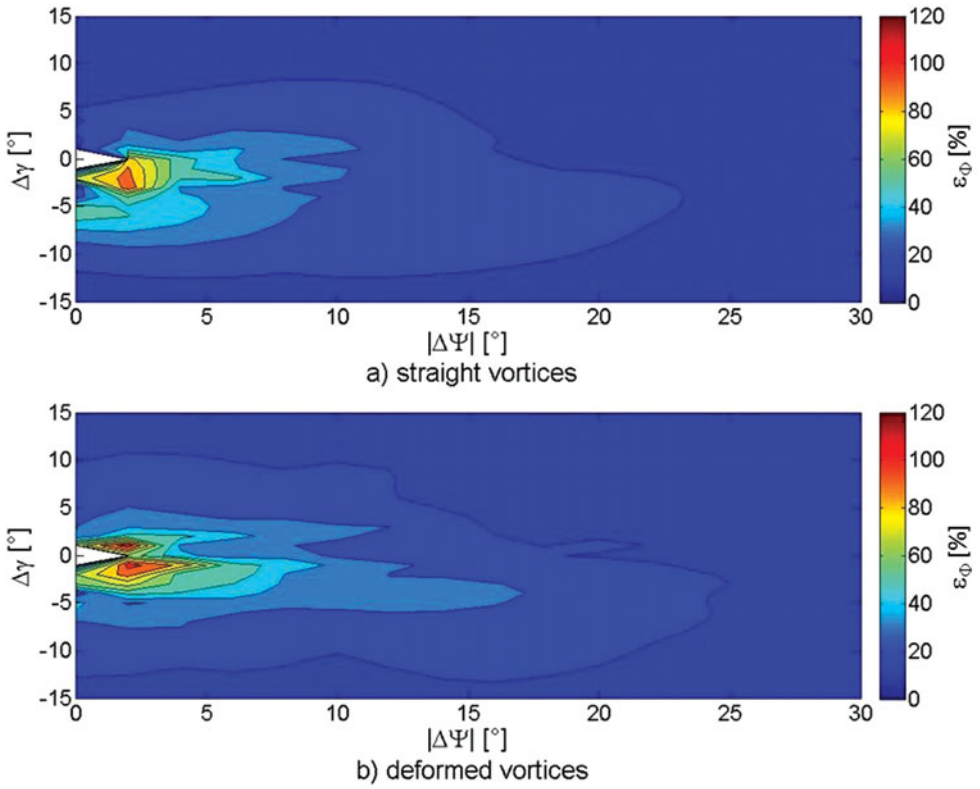

Figure 15. (Colour online) Comparison of maximum bank angle relative to maximum bank angle with straight vortices ($t_{age} = 16$ s, $t^* = 0.51$).

reference for the following figures (the 100%) is the strongest encounter with straight vortices of the respective vortex age and for the specific parameter. Therefore, the upper parts of the figures showing the results for straight vortices cannot exceed 100%, whereas the lower part showing the results for deformed vortices can exceed 100% in cases where the worst-case encounter with deformed vortices is stronger than the one with straight vortices. This way, differences between encounters with straight and deformed vortices are very obvious. The relation factor ε depicted in the following figures are calculated with:

$$\varepsilon_\Phi = \frac{\Phi_{\text{max, deformed}}}{\Phi_{\text{max, straight}}} \times 100 \quad \ldots (11)$$

$$\varepsilon_p = \frac{p_{\text{max, deformed}}}{p_{\text{max, straight}}} \times 100 \quad \ldots (12)$$

$$\varepsilon_n = \frac{n_{z,\text{max, deformed}}}{n_{z,\text{max, straight}}} \times 100 \quad \ldots (13)$$

In all the following figures, the combination of encounter angles of 0°/0° is disregarded, as in this case the aircraft is inside the vortices at the beginning of the simulation. This case is considered to be unrealistic, because in reality the aircraft would always approach this position

https://doi.org/10.1017/aer.2016.14 Published online by Cambridge University Press

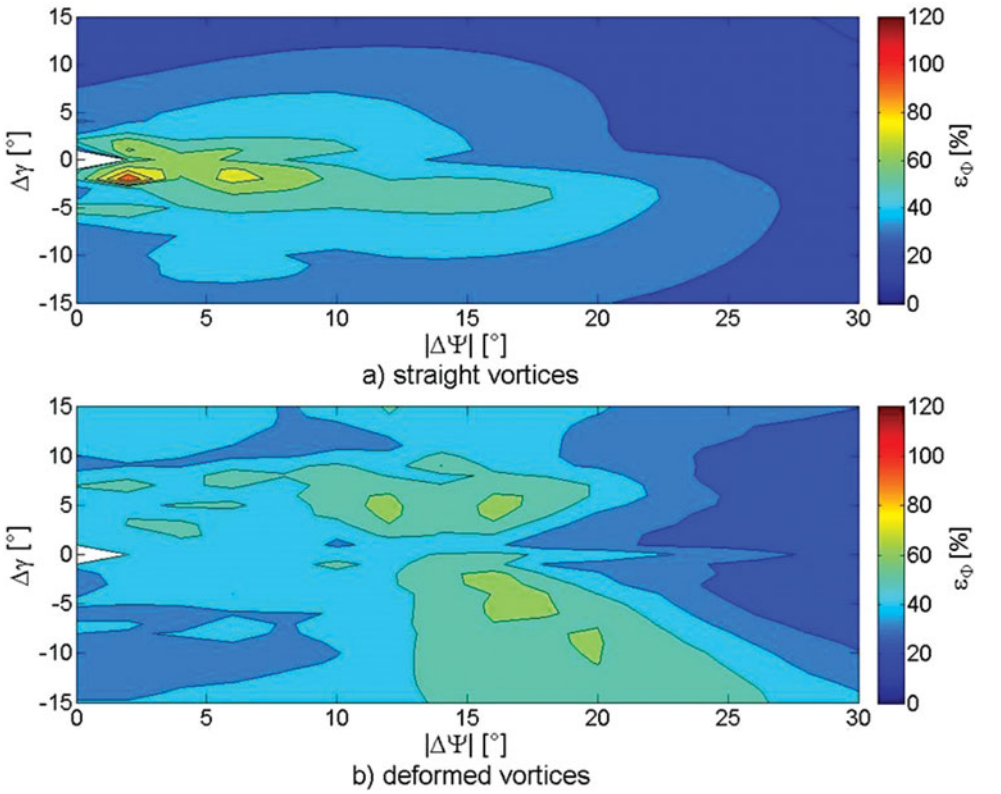

Figure 16. (Colour online) Comparison of maximum bank angle relative to maximum bank angle with straight vortices ($t_{age} = 108$ s, $t^* = 3.42$).

from outside the vortices, which means that the aircraft is always exposed to the vortex impact before reaching this position.

Figure 15 clearly shows the very similar distribution of maximum bank angles in the angular space between encounters with straight and deformed vortices for a vortex age of 16 seconds. This could be expected due to the fact that the vortices are very similar indeed. The results depicted in Fig. 15 are congruent with the common experience that for straight vortices, the largest aircraft response can be expected at shallow encounter angles when the aircraft approaches the vortices from slightly below. In this case, the impact of the first vortex changes the flight path in a way that the second vortex is hit very closely, resulting in a strong aircraft response (Fig. 12).

With increasing age, the deformation evolves and the shape of the vortex line differs increasingly between straight and deformed vortices. Figure 16 shows the distribution of maximum bank angles for a vortex age of 108 seconds. At such an age, the sinusoidal shape of the vortices is fully developed and the vortices are close to linking (Fig. 5). One can clearly observe in Fig. 16 that the maximum bank angle, which occurs during encounters with deformed vortices, is about 70-80% of the maximum bank angle of encounters with straight vortices. Thus, regarding the bank angle, encounters with wavy vortices result in less upset than with straight vortices. However, Fig. 17 shows that the resulting roll rate is much stronger during encounters with deformed vortices. The maximum roll rate with deformed

https://doi.org/10.1017/aer.2016.14 Published online by Cambridge University Press

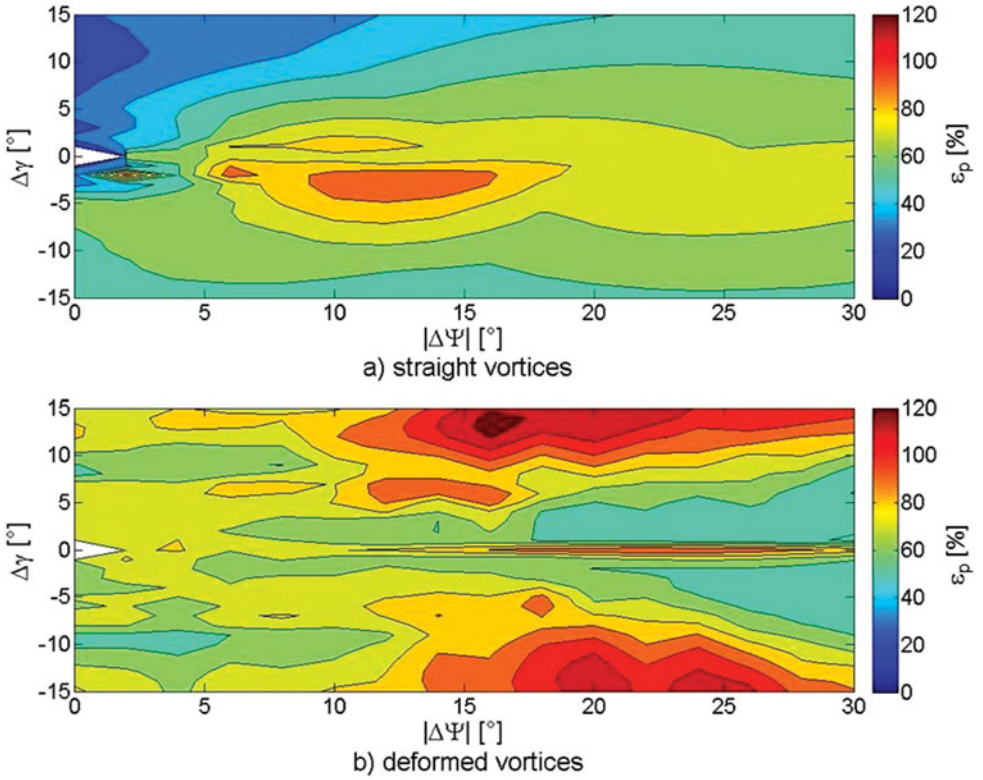

Figure 17. (Colour online) Comparison of maximum roll rate relative to maximum roll rate with straight vortices ($t_{age} = 108$ s, $t^* = 3.42$).

vortices is at about 120% of the maximum roll rate with straight vortices. Figures 16 and 17 indicate that encounters with wavy vortices are more abrupt. As can be seen in Fig. 10, the maximum RCR is larger during encounters with wavy vortices (at a vortex age of 108 s). This indicates that larger rolling moments are induced during the encounter, which lead to larger roll accelerations and thus larger roll rates. However, due to the vortex deformation, the encountering aircraft remains only briefly in close vicinity of the vortex core where the largest rolling moments are induced. Therefore, the bank angle cannot develop as much as during encounters with straight vortices, which are less rapid.

Another remarkable effect of vortex deformation can be observed in Figs. 16 and 17, namely a shift of the largest aircraft response towards greater values for the encounter angles $\Delta\gamma$ and $\Delta\Psi$. Both figures show that with straight vortices, the maximum aircraft response occurs at very shallow encounter angles (below $\pm 10°$ in azimuth and below $\pm 5°$ in encounter inclination for the maximum bank angle; $\pm 10°$ in inclination and ± 5 to $\pm 20°$ in azimuth respectively for roll rate). With deformed vortices, the area with the maximum aircraft response is shifted towards larger encounter angles (azimuth by about 15-20° for the bank angle and approximately 15-30° for the roll rate). This fact can be explained with the additional inclination of the vortex line due to the deformation, which leads to a change of the local encounter angles. This means that due to the deformation, the aircraft hits the vortex line under locally different angles than the globally defined encounter angles $\Delta\gamma$ and $\Delta\Psi$ (Fig. 9).

https://doi.org/10.1017/aer.2016.14 Published online by Cambridge University Press

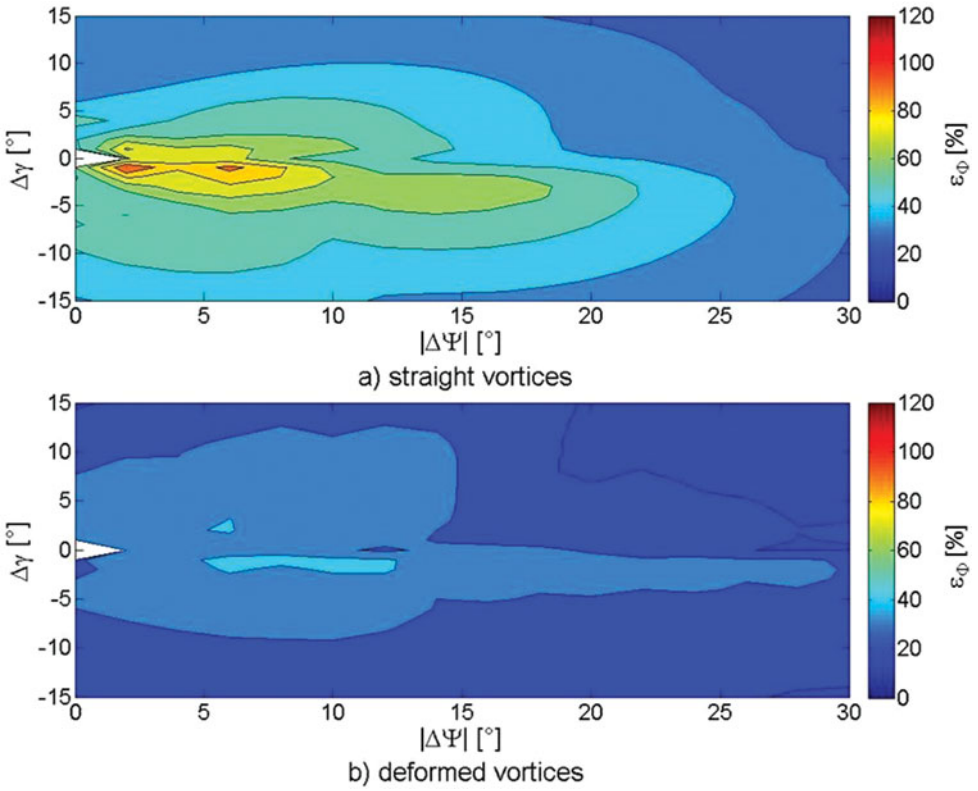

Figure 18. (Colour online) Comparison of maximum bank angle relative to maximum bank angle with straight vortices ($t_{age} = 136$ s, $t^* = 4.31$).

Figure 10 shows that the aircraft reaction is much smaller after the vortex linking. Vortex rings still have a considerable circulation but the strong deformation of the vortex line results in a weakening of the vortex impact due to the even shorter duration of the impact compared to wavy vortices. This can also be observed in Figs. 18 and 19, which again show the maximum bank angle and the maximum roll rate of encounters with a 136-second-old vortex in the stage of vortex rings (Fig. 5). One can observe in the figures that the maximum bank angle during encounters with deformed vortices is only at about 40% of the maximum bank angle with straight vortices of the same strength. Contrary to the stage of wavy vortices the roll rate shows the same tendency as for the bank angle with vortex rings. The maximum roll rate is much smaller as well with vortex rings (about 50-60% of straight vortices). In this stage of deformation, the duration of the rolling moment impact is too small for a considerable aircraft response in the roll axis. The results indicate that encounters with vortex rings are less roll-dominated than encounters with wavy or straight vortices. This was previously demonstrated in in-flight simulations performed with the former DLR research aircraft ATTAS[9].

Another issue for encounters with vortex rings is the vertical load factor. Figure 20 illustrates the maximum vertical load factor deviations that occurred during the vortex ring encounters. While the figure shows a distinct area of encounter angles with large load factors for straight vortices, large load factors also occurred with vortex rings over the whole range

https://doi.org/10.1017/aer.2016.14 Published online by Cambridge University Press

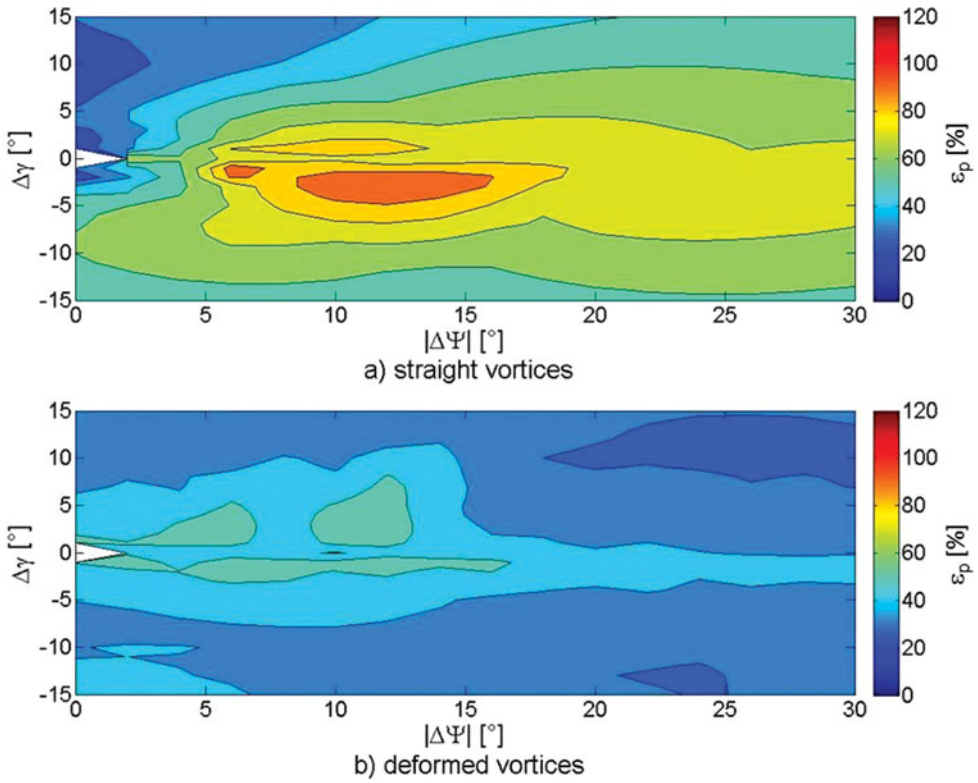

Figure 19. (Colour online) Comparison of maximum roll rate relative to maximum roll rate with straight vortices ($t_{age} = 136$ s, $t^* = 4.31$).

of encounter angles analysed. The circulation of the vortices generally keeps on decreasing after the vortex ring formation. However, in the areas of the vortex rings, perpendicular to the flight direction of the generator aircraft the circulation remains high for a longer period of time[13]. As a result, encounters with vortex rings are mostly not roll-dominant (due to the short duration of the single vortex impact), despite the fact that the flow field still comprises areas of considerable upwash or downwash. Therefore, encounters with vortex rings result in aircraft upsets comparable to strong turbulence. This was also previously experienced during the in-flight simulation campaign with ATTAS[9]. However, the author does not wish to give the impression that encounters with vortex rings are harmless or that they cannot pose a threat to the encountering aircraft, as the experience gained in recent studies shows that vortex rings should not be disregarded[9].

4.0 CONCLUSIONS

A simulation study was conducted in order to analyse differences between wake encounters with idealised straight vortices and realistically shaped deformed vortices. For this purpose, a parameter variation study was performed using the DLR ATRA aircraft simulation model and flow field data for the deformed vortices that were derived from large-eddy simulations (LES). For comparison, encounters with straight vortices were simulated with a simple model applying the Burnham-Hallock radial distribution of tangential velocity. The parameters

https://doi.org/10.1017/aer.2016.14 Published online by Cambridge University Press

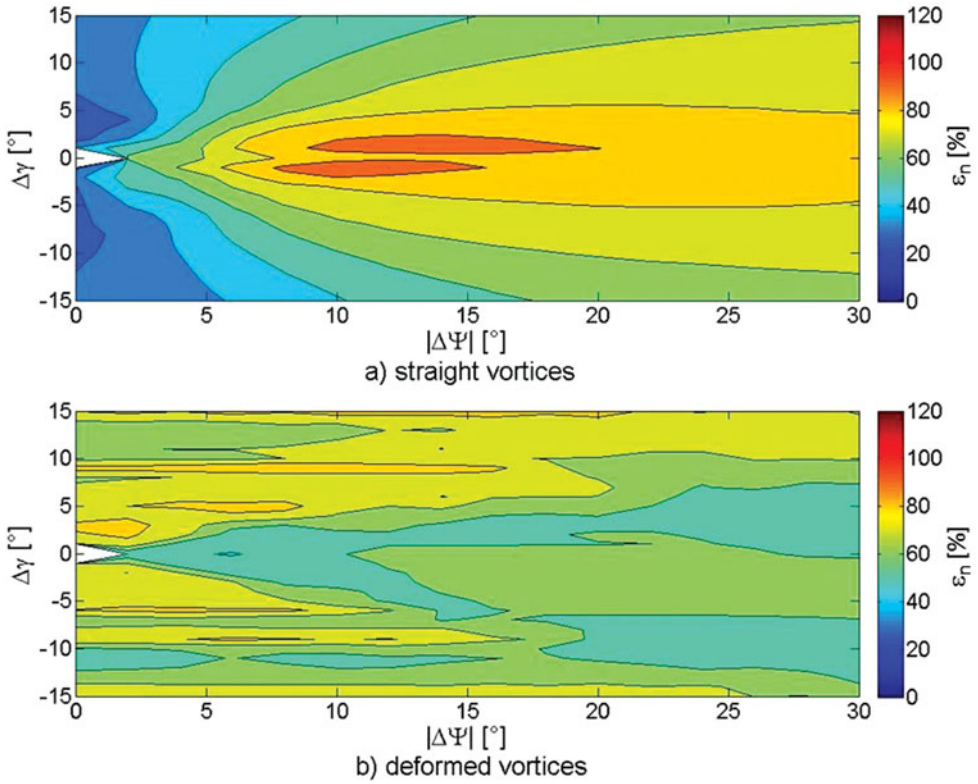

Figure 20. (Colour online) Comparison of maximum vertical load factor relative to maximum vertical load factor with straight vortices ($t_{age} = 136$ s, $t^* = 4.31$).

varied included the encounter angles and the encounter positions so that all possible encounter situations could be considered. The simulations were performed using vortices of nine different vortex ages comprising different stages of vortex deformation from nearly straight, followed by wavy vortices, and finally leading to vortex rings. In order to enable a correct comparison between straight and deformed vortices, the mean circulation of the LES-derived vortices was taken for the straight vortex model, allowing similar vortex strengths.

The simulations revealed that on average, encounters with deformed vortices were weaker than those with straight vortices independent of the vortex age. Furthermore, the maximum aircraft response was smaller for deformed vortices than with straight ones during encounters with young vortices, which were still nearly straight, and also with strongly deformed vortices after the linking phase of the vortex rings as well. However, the simulations also revealed that under certain conditions with wavy vortices shortly prior to linking, the aircraft response is larger than that for straight vortices. Such encounters did not result in larger bank angles but in larger roll rates and load factors. Hence, such encounters could be considered more hazardous. The analysis of the simulation data demonstrated that the differences between encounters with straight and deformed vortices can be explained by the different vortex impact in terms of amplitude and duration of the impact caused by the deformation of the vortex line. The simulations also highlighted that strong encounters occurred less often with wavy vortices than for straight vortices. This implies that encounters with wavy vortices can actually be

https://doi.org/10.1017/aer.2016.14 Published online by Cambridge University Press

stronger. However, the probability of a strong encounter occurring is less than that for straight vortices.

This outcome could be relevant for all kinds of efforts in the area of revising the existing wake-vortex-related separation distances, as is currently ongoing within different projects worldwide. It should be considered from a safety perspective that a revision of separation distances might shift possible encounters from the stage of vortex rings towards wavy vortices, resulting in stronger encounters than expected when models of straight vortices are used for hazard analysis.

REFERENCES

1. N.N. Procedures for Air Navigation Services, Air traffic management, *ICAO Doc*, 2007, **4444**, (15), pp 6-12.
2. N.N. Data Show That U.S. Wake-turbulence Accidents Are Most Frequent at Low Altitude and During Approach and Landing, Flight safety digest, *Flight Safety Foundation*, 2002, **21**, (3-4), pp 1-47.
3. HAHN, K.-U. and SCHWARZ, C.W. Wake vortex avoidance versus landing capacity, AIAA Paper 2006-6322, AIAA Guidance, Navigation, and Control Conference, 2006, Keystone, Colorado, US.
4. DONOHUE, G.L. and RUTISHAUSER, D.K. The effect of aircraft wake vortex separation on air transportation capacity, 4 FAA/Eurocontrol R&D Conference, 2001, Santa Fe, New Mexico, US.
5. LUCKNER, R. Modeling and simulation of wake vortex encounters: state-of-the-art and challenges, AIAA Paper 2012-4633, AIAA Modeling and Simulation Technologies Conference, 2012, Minneapolis, Minnesota, US.
6. CROW, S.C. Stability theory for a pair of trailing vortices, *AIAA J*, 1970, **8**, (12), pp 2172-2179.
7. CROW, S.C. and BATE, E.R. Lifespan of trailing vortices in a turbulent atmosphere, *J Airc*, 1976, **13**, (7), pp 476-482.
8. LOUCEL, R.E. and CROUCH, J.D. Flight-simulator study of airplane encounters with perturbed trailing vortices, AIAA Paper 2004-1074, 42nd AIAA Aerospace Sciences Meeting and Exhibit, 2004, Reno, Nevada, US.
9. VECHTEL, D. In-flight simulation of wake encounters using deformed vortices, *Aeronautical J*, October 2013, **117**, (1196), pp 997-1018.
10. VECHTEL, D. Flight simulator study on the influence of vortex curvature on wake encounter hazard using LES wind fields, *Aeronautical J*, 2012, **116**, (1177), pp 287-302.
11. BIENIEK, D. and LUCKNER, R. Simulation of aircraft encounters with perturbed vortices considering unsteady aerodynamic effects, AIAA Paper 2012-4657, *AIAA Atmospheric Flight Mechanics Conference*, 2012, Minneapolis, Minnesota, US.
12. RAAB, C. Flugdynamisches Simulations modell A320-ATRA—Validierungsversuche und Bewertung der Modellgüte (English: Flight dynamics simulation model A320-ATRA—validation tests and rating of model accuracy), DLR Internal Report IB 111-2012/43, 2012, Braunschweig, Germany.
13. HENNEMANN, I. Deformation und Zerfall von Flugzeugwirbelschleppen in turbulenter und stabil geschichteter Atmosphäre (English: deformation and decay of aircraft wake vortices in turbulent and stable stratified atmosphere), Dissertation, Technical University Munich, 2010, Germany.
14. FISCHENBERG, D. A method to validate wake vortex encounter models from flight test data, ICAS 2010, 27th International Congress of the Aeronautical Sciences, 2010, Nice, France.
15. N.N. manual of criteria for the qualification of flight simulation training devices, *ICAO Doc*, 2009, **9625**, (3).
16. N.N. A320 flight crew operating manual, Part I, System Description, Issue 01 December 2008.
17. N.N. A320/A321 aircraft maintenance manual AMM, Reference DG. AMM AEF, Issue 01, May 2009.
18. BURNHAM, D. and HALLOCK, J. Chicago monostatic acoustic vortex sensing system 4, *Wake Vortex Decay, National Information Service*, 1982, Springfield, Virginia, US.
19. ROSENHEAD, L. The formation of vortices from a surface of discontinuity, *Proceedings Royal Society of London, Ser. A*., 1932, **134**, pp 170-192.

https://doi.org/10.1017/aer.2016.14 Published online by Cambridge University Press

20. FISCHENBERG, D. Bestimmung der Wirbelschleppencharakteristik aus Flugmessdaten (English: determination of wake vortex characteristics from flight test data), *German Aerospace Congress*, 2002, Stuttgart, Germany.
21. SCHWARZ, C.W. and HAHN, K.-U. Full-flight simulator study for wake vortex hazard area investigation, *Aerospace Science and Technology*, 2006, **10**, (2), pp 136-143.
22. GERZ, T. and SCHWARZ, C. Das DLR-Projekt "Wetter und Fliegen" (English: the DLR project "weather and flying"), DLR Research Report 2012-02, 2012, Oberpfaffenhofen, Germany.
23. FRECH, M. *et. al*. High-resolution weather database for the terminal area of Frankfurt Airport, *J Applied Meteorology and Climatology*, 2007, **46**, (11), pp 1913-1932.
24. BARROWS, T.M. Simplified methods of predicting aircraft rolling moments due to vortex encounters, AIAA Paper 76-61, AIAA 14th Aerospace Sciences Meeting, 1976, Washington, DC, US.
25. DE BRUIN, A. WAVENC, wake vortex evolution and wake vortex encounter, Publishable Synthesis Report, National Aerospace Lab., NLR-TR-2000-079, 2000, Amsterdam, The Netherlands.
26. JATEGAONKAR, R., FISCHENBERG, D. and GRUENHAGEN, W.V. Aerodynamic modelling and system identification from flight data – recent applications at DLR, *J Airc*, 2004, **41**, (4), pp 687.
27. HAHN, K.-U. and SCHWARZ, C.W. Safe limits for wake vortex penetration, AIAA Paper 2007-6871, AIAA Guidance, Navigation and Control Conference and Exhibit, 2007, Hilton Head, South Carolina, US.

https://doi.org/10.1017/aer.2016.14 Published online by Cambridge University Press